COMMUNICATIONS IN COMPUTATIONAL PHYSICS
Vol. **4**, No. 5, pp. 1129-1150

Commun. Comput. Phys.
November 2008

Progress of Pattern Dynamics in Plasma Waves

B. Qiao[1,2,3], C. T. Zhou[3,4,5,*], X. T. He[3,4,5] and C. H. Lai[2,6]

[1] *Center for Plasma Physics, Department of Physics and Astronomy, Queen's University Belfast, Belfast BT7 1NN, UK.*
[2] *Department of Physics, National University of Singapore, Singapore 117542.*
[3] *Institute of Applied Physics and Computational Mathematics, P. O. Box 8009, Beijing 100088, China.*
[4] *Center for Applied Physics and Technology, Peking University, Beijing 100871, China.*
[5] *Institute for Fusion Theory and Simulation, Zhejiang University, Hangzhou 310027, China.*
[6] *Beijing-Hong Kong-Singapore Joint Centre for Nonlinear & Complex Systems (Singapore), National University of Singapore, Singapore 117542.*

Received 29 February 2008; Accepted (in revised version) 8 July 2008

Available online 9 September 2008

Abstract. This paper is concerned with the pattern dynamics of the generalized nonlinear Schrödinger equations (NSEs) related with various nonlinear physical problems in plasmas. Our theoretical and numerical results show that the higher-order nonlinear effects, acting as a Hamiltonian perturbation, break down the NSE integrability and lead to chaotic behaviors. Correspondingly, coherent structures are destroyed and replaced by complex patterns. Homoclinic orbit crossings in the phase space and stochastic partition of energy in Fourier modes show typical characteristics of the stochastic motion. Our investigations show that nonlinear phenomena, such as wave turbulence and laser filamentation, are associated with the homoclinic chaos. In particular, we found that the unstable manifolds $W^{(u)}$ possessing the hyperbolic fixed point correspond to an initial phase $\theta=45^\circ$ and 225°, and the stable manifolds $W^{(s)}$ correspond to $\theta=135^\circ$ and 315°.

PACS: 47.54.-r, 05.45.Yv, 52.25.Gj, 52.35.Mw
Key words: Pattern dynamics, homoclinic chaos, nonlinear Schrödinger equations, plasma waves.

1 Introduction

It is well known that the generalized nonlinear Schrödinger equation (NSE) [1–25] is of the form

$$iE_t+\partial_x^2E+F(|E|^2)E=0, \tag{1.1}$$

*Corresponding author. *Email addresses:* b.qiao@qub.ac.uk (B. Qiao), zcangtao@iapcm.ac.cn (C. T. Zhou), xthe@iapcm.ac.cn (X. T. He), phylaich@nus.edu.sg (C. H. Lai)

where $E(x,t)$ is the complex amplitude of waves, and t and x are time and space variables, respectively. The function F is used to describe different physical processes [20–23], such as plasma physics, nonlinear optics, fluid dynamics, superconductivity theory and Bose-Einstein condensates (BEC) etc. The generalized NSE is one of the basic evolution models for nonlinear process in various branches of the conservative systems. Early applications of the NSE were in the context of nonlinear optics where it described the propagation of light beams in nonlinear media [24]. Also it has been applied to gravity waves on deep water, for which the predicted modulational instability and envelope soliton formation have been clearly demonstrated experimentally [25]. In plasma physics, a large number of nonlinear processes, such as nonlinear hydromagnetic waves [26], small-K condensation of weak turbulence in nonlinear plasmas, Langmuir waves in electrostatic plasmas, femtosecond (fs) laser pulse in air, medium-intensity laser in underdense plasma and intense laser pulse in relativistic plasmas, can all be effectively modeled by the generalized NSE (1.1) with different potential function F.

For the generalized NSE (1.1), the Lagrangian density is

$$L=\frac{i}{2}(E^*E_t-EE_t^*)-|E_x|^2+f(|E|^2), \tag{1.2}$$

where $f(|E|^2)=\int_0^{|E|^2}F(s)ds$. The system described by it is a conservative system. According to the Norther theorem, we can obtain the following invariants: the quasiparticle number

$$N=\int|E|^2dx, \tag{1.3}$$

the momentum

$$P=i\int E^*E_xdx, \tag{1.4}$$

and the Hamiltonian quantity

$$H=\int[|E_x|^2-f(|E|^2)]dx. \tag{1.5}$$

For such a conservative Hamiltonian system (1.1) or (1.2), the nonlinear dynamics including solitary waves and patterns are very important. In nature, most nonlinear phenomena, such as Langmuir wave collapse, laser self-focusing and filamentation, are all associated with the basic nonlinear dynamics of the system and are the results of nonlinear development of modulational instability. However, the latter has not been systematically studied, while previous work has concentrated on the solitary wave solutions and the singular solutions. The study of complex dynamics including chaos and patterns for the generalized NSE (1.1) associated with different physical problems is of interest to the understanding of various nonlinear phenomena in plasmas.

In 1992, we found for the first time that an one-dimensional cubic-quintic nonlinear Schrödinger equation [1, 2] is non-integrable [3] due to high-order Hamiltonian perturbation. Physically, our results showed that the coherent pattern of plasma electron (Langmuir) waves can be broken down due to high-order field interaction of Langmuir waves and ion-acoustic waves. Then we completed some systematic investigations on pattern dynamics of the generalized nonlinear Schrödinger equations [4–12], Zakharov equations [13–15] and complex Ginzburg-Landau equations [16, 17] in one- and two-dimensional spaces, respectively. Our investigations showed that nonlinear phenomena, such as wave turbulence and laser filamentation, etc., are associated with the homoclinic chaos. In particular, we found that the unstable manifolds $W^{(u)}$ possessing the hyperbolic fixed point correspond to an initial phase $\theta=45^\circ$ and 225°, and the stable manifolds $W^{(s)}$ correspond to $\theta=135^\circ$ and 315°. Recently, we have applied our method to investigate complex dynamics of femtosecond terawatt laser pulses in air [18] and relativistic lasers in plasmas [19]. Our investigations further show that our previously theoretical methods and numerical strategies are applicable for the study of different physical systems. Pattern dynamics in nonequilibrium system [27], in nonlinear optics [28], and in chemical systems [29] have been all reviewed. This paper mainly covers pattern dynamics of the generalized nonlinear Schrödinger equations related to various nonlinear physical problems in plasmas.

The paper is organized as follows. In Section 2, we give a qualitative nonlinear analysis of NSE (1.1) and constitute an available phase space and initial condition to describe its nonlinear behavior. In Sections 3-7, we analyze the dynamics in detail respectively of cubic NSE (CNSE) for weak turbulence in plasmas, quintic NSE for langmuir waves in plasmas, higher-order NSE for fs laser pulse in air, exponential NSE for medium-intensity laser in underdense plasmas and relativistic NSE (RNSE) for intense laser in relativistic plasmas. Some conclusion and discussion are given in Section 8.

2 Qualitative analysis

For the continuum Hamiltonian system (1.1) or (1.2), the dynamic description is dependent on the choice of the initial condition. In particular, we cannot give a reasonable explanation if we take an arbitrary initial condition. Therefore, it is necessary that we choose an available initial condition and constitute a reasonable phase space in order to discuss the nonlinear evolution properties of this system. For definitiveness, we only deal with the developing behavior of an initial homogeneous state due to the modulational instability. In other words, we consider the nonlinear modulation of the plane wave solution as in [3]

$$E_s(t)=E_0\exp(i\lambda t), \tag{2.1}$$

where $\lambda=F(|E_0|^2)$ for $E_0\neq 0$.

In the presence of small perturbations, we can write

$$E(x,t)=E_s(t)+\delta E(x,t), \tag{2.2}$$

where $\delta E(x,t) \ll E_s(t)$. Linearizing the NSE (1.1), we obtain the eigen equation for the perturbation field $\delta E(x,t)$ as

$$\begin{pmatrix} i\partial_t+\partial_x^2+L & L \\ L & -i\partial_t+\partial_x^2+L \end{pmatrix}\begin{pmatrix} \delta E \\ \delta E^* \end{pmatrix}=0, \tag{2.3}$$

where $L=F'(|E_0|^2)|E_0|^2$ and $F'(u)=\partial_u F$.

For periodic boundary conditions, the eigenfunction $\delta E(x,t)$ can be defined [3–12] as

$$\begin{pmatrix} \delta E \\ \delta E^* \end{pmatrix}=\begin{pmatrix} \epsilon\exp(i\mu t) \\ \epsilon^*\exp(-i\mu^* t) \end{pmatrix}\cos(kx), \tag{2.4}$$

where ϵ and ϵ^* are small parameters, and k is the wave number of the perturbation. Some algebra yields the eigenvalue [5]

$$\mu=2\left[F'(|E_0|^2)|E_0|^2-k^2\right]\pm i\sqrt{k^2\left[2F'(|E_0|^2)|E_0|^2-k^2\right]}, \tag{2.5}$$

and the growth rate

$$\Gamma=\mathrm{Im}(\mu)=\sqrt{k^2\left[2F'(|E_0|^2)|E_0|^2-k^2\right]}. \tag{2.6}$$

The wave number of the most unstable mode is then $K_{max}=\sqrt{f'(|E_0|^2)|E_0|^2}$. Inserting Eqs. (2.4) and (2.5) into Eq. (2.3), we easily obtain that [3]

$$\delta E/\delta E^*=\pm i. \tag{2.7}$$

To analyze the nonlinear behavior of the system (1.1), we construct phase space ($|E|$, $d_t|E|$) at $x=0$ [10, 11, 13, 30]. From Eq. (2.5), we see that the eigenvalue μ has a pair of conjugated complex roots, thus we can determine that $(E_0,0)$ is associated with a saddle (or hyperbolic fixed) point in phase space [3]. Furthermore, from Eq. (2.4) the initial condition can be chosen as

$$E(x,0)=E_0+\eta\exp(i\theta)\cos(k_x x). \tag{2.8}$$

We therefore find that the unstable manifolds $W^{(u)}$ possessing the hyperbolic fixed point correspond to $\theta=45^\circ$ and 225°, and the stable manifolds $W^{(s)}$ correspond to $\theta=135^\circ$ and 315° [3–12].

3 Cubic NSE for coherent solitons in plasmas

The dynamical structure of Hamiltonian systems is sensitive to initial conditions [31–33]. The analysis above gives us a practical initial condition as well as a suitable phase space for describing the nonlinear behavior of the system that can be described by the

generalized NSE (1.1). Using such an initial condition and phase space, we can study various physical systems, once its potential function F in NSE (1.1) is determined.

First, for the cubic NSE (CNSE), the potential function is taken as

$$\text{(i)} \qquad F(|E|^2)=\alpha|E|^2, \tag{3.1}$$

where α is a parameter and the Hamiltonian can be written as

$$H_0=\int\left(|E_x|^2-\frac{1}{2}\alpha|E|^4\right)dx, \tag{3.2}$$

which is integrable. The cubic NSE has been widely studied in nonlinear optics and fibers etc. [34,35]. Recently, the stabilization of high-order solutions of the cubic NSE has been discussed [36]. In nonlinear plasmas, it describes the nonlinear interaction between Langmuir wave and ion-acoustic wave in the subsonic regime, where the interaction of the second-order fields is only considered. In the initial stages of field evolutions, many physical phenomena, such as solitons developed by modulational instabilities, can be explained in terms of this model.

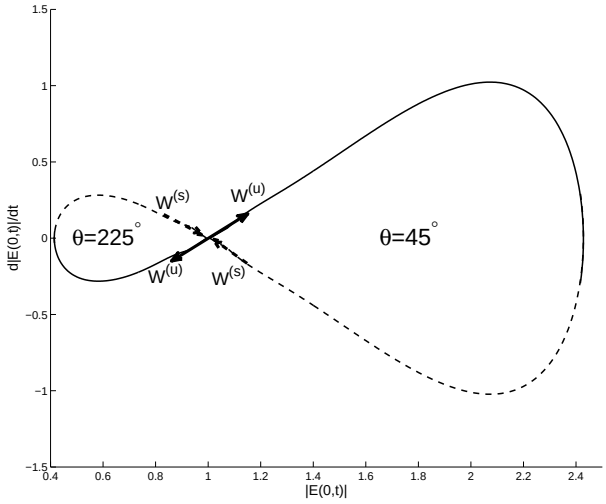

Figure 1: Stable $W^{(s)}$ and unstable $W^{(u)}$ manifolds of the hyperbolic fixed point $(E_0,0)$ with $\theta=45^\circ$ and 225° for the CNSE [Eq. (1.1) combined with Eq. (3.1)], where the solid curve is computed with $t>0$ and the dashed curve is computed with $t<0$.

In [10], we gave the solution of the CNSE [Eqs. (1.1) and (3.1)] by taking the initial condition (2.8) and choosing $E_0=1$, $\alpha=1$, $\eta=0.1$, $\theta=45^\circ$ and 225° respectively. The standard splitting-step spectral method [3,10,11] is improved [12] in order to better preserve the conserved quantities (1.3)-(1.5). The spatial period of the system is taken to be $L=2\pi/K_{max}$. From Fig. 1, we see the theoretical analysis in Section 2 is completely verified. The CNSE is fully integrable due to the existence of Lax pair, i.e., H_0 is integrable. One solution corresponding to the periodic oscillations is shown in Fig. 2. The

corresponding phase-space trajectory is a homoclinic orbit (HMO). The stable manifold smoothly joins the unstable manifold at the saddle point (E_0,0), i.e., HMO connection, and the well-known Fermi-Pasta-Ulam (FPU) recurrence exists, as shown in Fig. 2(b). The fundamental frequency of the periodic solution is shown in Fig. 2(c). Because of the exact FPU recurrence, a spatially coherent pattern appears, shown in Fig. 2(d).

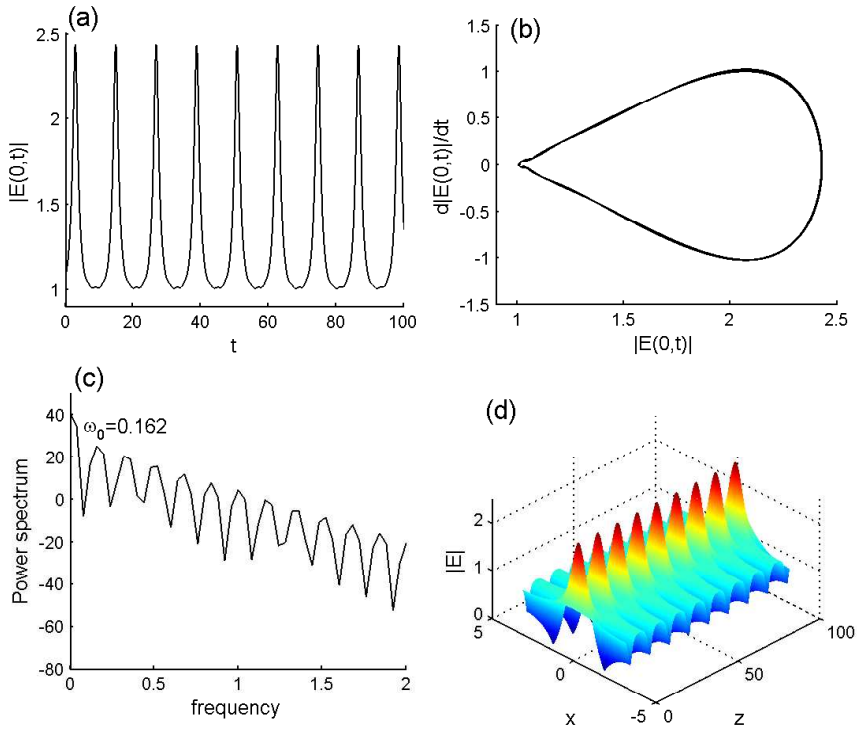

Figure 2: Dynamics of the CNSE [Eqs. (1.1) and (3.1)] for $E_0=1$, $\eta=0.1$ and $\theta=45°$. (a) the evolution of laser field envelope at $x=0$; (b) the trajectories of the phase space $(E(0,t),\ d|E(0,t)|/dt)$; (c) the corresponding power spectra; and (d) the corresponding spatial patterns.

To display this recurrence, the evolution of the energy contained in Fourier modes was measured. In Fourier space, the energy of the system is defined as

$$\mathcal{H}=\sum_n \mathcal{H}_{K_n}=\sum_n |E_{K_n}|^2, \tag{3.3}$$

and the initial energy is added to the mode K_{max}. From Fig. 3, we observe that a large part of the energy in the system lies in the first and second modes. Furthermore, the evolution of the energy in all modes is periodic, which is consistent with the periodic recurrence. This means that the unstable modulation first grows exponentially as predicted by Benjamin and Feir [37] but eventually the solution would demodulate and return to a near-uniform state. Thus, solitons developed by modulational instability keep their spatially coherent structures and temporally periodic evolutions.

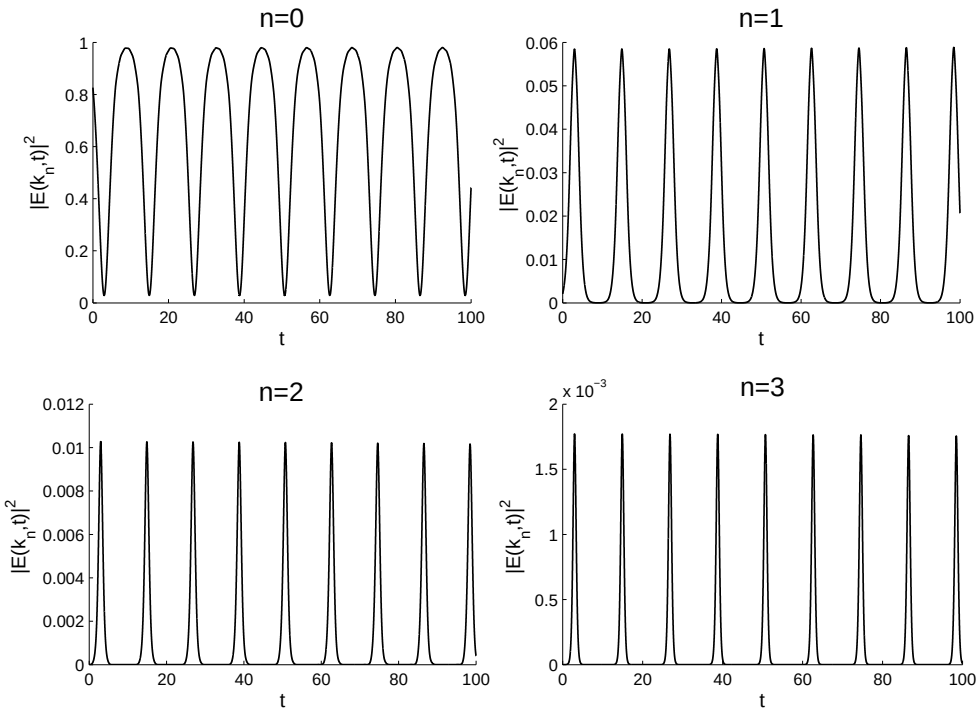

Figure 3: The energy evolution in the first four Fourier modes for the CNSE [Eqs. (1.1) and (3.1)], where the parameters are the same as Fig. 2.

4 Quintic NSE for Langmuir waves in electrostatic plasmas

For Langmuir waves in electrostatic plasmas, the beat-frequency interaction between large amplitude parts of high frequency fields and particles can occur in strong turbulent stage of plasma instability. The other physical effects, for example, damping and dissipation, have to be considered and the CNSE is no longer valid. Under the static approximation, from Vlasov-Maxwell equations, He [1] has obtained a quintic NSE describing the nonlinear interaction between Langmuir waves and electrons in plasmas, where the potential $F(|E|^2)$ can be expressed as

$$\text{(ii)} \qquad F(|E|^2)=|E|^2-g|E|^4, \tag{4.1}$$

where $E(x,t)$ is the slowly-varying complex amplitude of Langmuir wave fields, and g is the coupling constant of Langmuir wave fields with electrons, which depends on electron temperature and density, etc. The Hamiltonian of the quintic NSE [Eq. (1.1) combined with the potential (4.1)] can be written as

$$H=H_0+H_1, \tag{4.2}$$

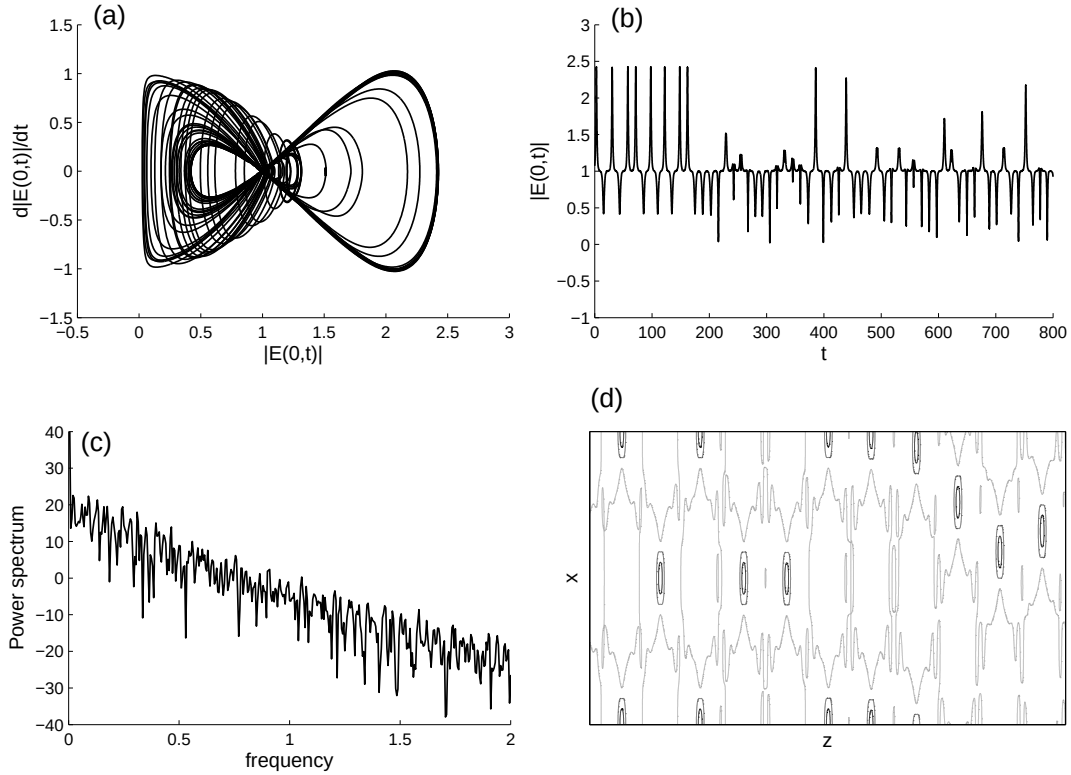

Figure 4: Dynamics of the quintic NSE [Eqs. (1.1) and (4.1)] for $E_0=1$, $\eta=0.1$ and $\theta=45^\circ$. (a) the trajectories of the phase space $(E(0,t),\, d|E(0,t)|/dt)$; (b) the evolution of laser field envelope at $x=0$; (c) the corresponding power spectra; and (d) the corresponding spatial patterns.

where H_0 is the one for the integrable CNSE [Eq. (3.2) with $\alpha=1$] and

$$H_1=\int \frac{1}{3}g|E|^6dx \tag{4.3}$$

acts as a quintic Hamiltonian perturbation to H_0.

Much attention has been focused on analyzing the behavior of high-order NSEs involving quintic terms [38, 39]. In 1992, we [3] systematically studied the dynamic properties of such quintic NSE for Langmuir waves in plasmas. We found that due to H_1, the NSE integrability is broken down and chaos and complex patterns of wave fields are formed. Fig. 4(a) clearly illustrates the chaotic behavior of the wave fields. Fig. 4(b) shows the presence of irregular HMO crossings, where the irregular motions appear nearby HMO. These demonstrate the presence of stochastic motions for complex dynamics. The power spectra [Fig. 4(c)] also clearly indicate the broadband structures and noiselike spectra being typical of chaotic evolutions. Fig. 4(d) shows that the Langmuir wave field patterns are no longer coherent but still keep their spatially localized struc-

tures. Physically, this means that the high-order nonlinear effects occurring during the long-term evolution of Langmuir waves in plasmas result in the conversion of wave field patterns from coherence to turbulence. Furthermore, the conversion is chaotic but keeps their spatially localized structures.

5 Higher-order NSE for femtosecond laser pulse in air

Propagation of femtosecond (fs) Terawatt (TW) laser pulses [23] in air has attracted wide interest due to its applications in lightning discharge control and atmospheric remote sensing [40–42]. Self-channeling of initial laser pulse experiences an early self-focusing (SF) stage caused by the Kerr response of air, which leads to a sharp increase of laser intensity. When laser intensity increases close to the ionization threshold, $\chi^{(5)}$ susceptibility originated from expansion of the nonlinear polarization vector and multiphoton ionization (MPI) of air molecules play important roles in the propagation dynamics [43].

Recently, we [18] applied the above method to investigate the complex dynamics of such laser pulses in air by considering the NSE (1.1) with the potential function

$$\text{(iii)} \qquad F(|E|^2)=\alpha|E|^2-\epsilon|E|^4-\gamma|E|^{2K}, \tag{5.1}$$

which includes Kerr focusing of air, $\chi^{(5)}$ susceptibility originated from expansion of nonlinear polarization, and plasma generation by MPI of air molecules. It is noted that the time variable t in Eq. (1.1) has been replaced with the propagation distance z for the following problems. For pulse duration $t_p=250$fs and wavelength $\lambda_0=800$nm, their coefficients take values $\alpha=0.446$, $\epsilon=7.3\times10^{-7}[\text{cm}^2/w_0^2]$ and $\gamma=8.4\times10^{-40}[\text{cm}^{2(K-2)}]/w_0^{2k-2}$ with w_0 laser beam transverse width in unit of cm. The variables z, x and E are normalized by the units of $4z_f$, w_0, and $\sqrt{P_{cr}/4\pi w_0^2}$, respectively, where $z_f=\pi w_0^2/\lambda_0$ is the Rayleigh length and $P_{cr}=2.55$GW the critical power for SF.

The Hamiltonian of such a NSE [Eqs. (1.1) and (5.1)] can also be written as Eq. (4.2), where

$$H_1=\int\left(\frac{1}{3}\epsilon|E|^6+\frac{1}{K+1}\gamma|E|^{2K+2}\right)dx. \tag{5.2}$$

If only the Kerr effect is considered, $H=H_0$ [Eq. (3.2)] is integrable corresponding to a CNSE. $\chi^{(5)}$ susceptibility and MPI effect act as a Hamiltonian perturbation H_1 to H_0. Fig. 5(a) gives comparisons of these three effects for different laser intensities I_0. For $I_0<10^{12}\text{W/cm}^2$, purely Kerr nonlinearity plays a major role with $H\approx H_0$ integrable. For $10^{12}<I_0<2\times10^{13}\text{W/cm}^2$, $\chi^{(5)}$ susceptibility starts to act as a small perturbation H_1. For $I_0>2\times10^{13}\text{W/cm}^2$, MPI appears, laser propagation is governed by all three effects with H nonintegrable. When I_0 further increases to larger than $5\times10^{13}\text{W/cm}^2$, MPI dominates $\chi^{(5)}$ susceptibility and laser beams reveal complex dynamics, including SF and filamentation.

Our numerical results given in Fig. 5(b) completely verify the theoretical analysis obtained in Section 2, where $W^{(u)}$ possessing the hyperbolic fixed point correspond to $\theta=45^\circ$ and 225°, and $W^{(s)}$ correspond to $\theta=135^\circ$ and 315°. Fig. 5(c) plots the unstable growth rate Γ for different I_0. From Figs. 5(c) and (a), we can understand that laser pulse with lower intensity ($I_0<10^{12}\mathrm{W/cm^2}$) follows the early SF caused by purely Kerr response of air, which compresses laser beam in the transverse plane and increases the intensity sharply [see Fig. 5(c), Γ is very large for $I_0=10^{11}\mathrm{W/cm^2}$]. With increasing I_0, both $\chi^{(5)}$ susceptibility and MPI become important mechanisms, the growth of laser field amplitude is quickly arrested by such two effects [see Fig. 5(c), Γ much decreases when I_0 increases, in particular, for $I_0=3\times10^{13}\mathrm{W/cm^2}$].

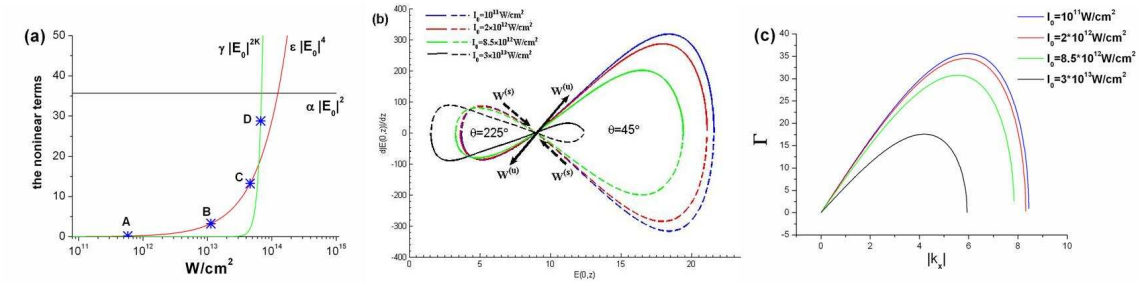

Figure 5: (a) Comparison of three nonlinear effects for different I_0 in Eq. (5.1). Asterisk symbols mark the points with I_0 respectively of 5.82×10^{11}, 1.13×10^{13}, 4.6×10^{13} and $6\times10^{13}\mathrm{W/cm^2}$. (b) Stable $W^{(s)}$ and unstable $W^{(u)}$ manifolds for the saddle point $(E_0,0)$ with $\theta=45^\circ$ and 225°, where the solid curve is calculated by NSE's (1.1) and (5.1) with $z>0$ and the dashed curve with $z<0$. (c) The growth rate Γ with the corresponding I_0.

We choose input laser power $P_{in}=10P_{cr}$ ($E_0=8.94$) with noise level 0.01 ($\eta=0.089$), initial phase $\theta=45^\circ$, and consider the most unstable mode with $k=K_{max}$. Initial laser intensities $I_0=10^{11}$, 3×10^{12}, 8.5×10^{12} and $3\times10^{13}\mathrm{W/cm^2}$ are considered, respectively. Figs. 6 and 7 plot the solutions. For $I_0=10^{11}\mathrm{W/cm^2}$, as analyzed above, the laser propagation obeys an integrable CNSE with only Kerr effect. Laser fields reveal periodic oscillation with the maximum intensity $I_{max}=5.82\times10^{11}\mathrm{W/cm^2}$ [see Fig. 6(a) and point "A" in Fig. 5(a)]. The phase trajectory is a HMO connection [see Fig. 6(b)]. Fig. 7(a) shows its spatially coherent pattern structure of the laser fields.

When I_0 increases to greater than $10^{12}\mathrm{W/cm^2}$, $\chi^{(5)}$ susceptibility and MPI play roles as a Hamiltonian perturbation H_1, we see from Figs. 6(d)-(l) that HMO connection is broken down, laser fields oscillate aperiodically and irregular motions appear. For $I_0=2\times10^{12}\mathrm{W/cm^2}$, we see in Fig. 6(d) that laser fields oscillate quasi-periodically with $I_{max}=1.13\times10^{13}\mathrm{W/cm^2}$, where $\chi^{(5)}$ susceptibility starts to act [see point "B" in Fig. 5(a)]. Fig. 6(e) shows the typical weak chaotic behavior [31]: the phase trajectory is a band, the KAM torus has a small thickness but is not completely broken down. Fig. 7(b) shows that laser field pattern structure still remains fairly coherent, but irregular sub-structures appear.

For $I_0=8.5\times10^{12}$ and $3\times10^{13}\mathrm{W/cm^2}$, laser fields oscillate aperiodically with respectively $I_{max}=4.6\times10^{13}$ and $6\times10^{13}\mathrm{W/cm^2}$ [see Figs. 6(g) and (j)], MPI effect appears [see point "C" in Fig. 5(a)] and dominates [see point "D"], it combined with $\chi^{(5)}$ susceptibil-

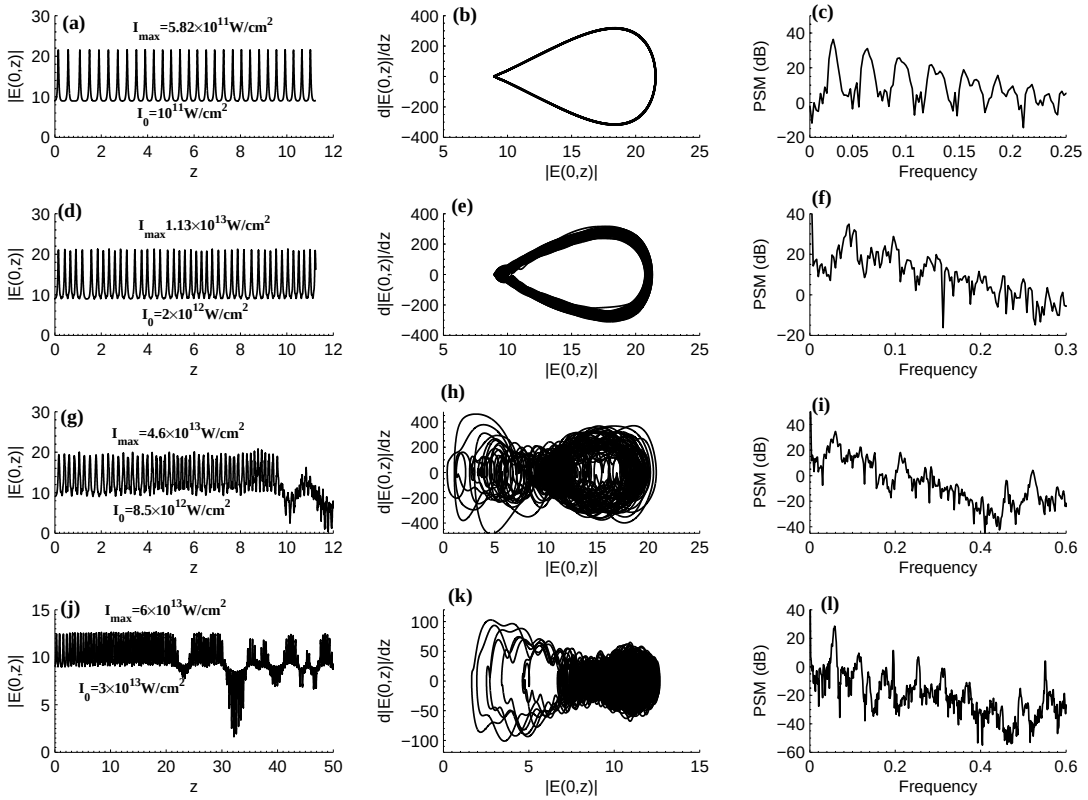

Figure 6: Complex dynamics of laser fields in air with I_0 respectively of 10^{11} [(a)-(c)], 2×10^{12} [(d)-(f)], 8.5×10^{12} [(g)-(i)] and $3\times10^{13}\mathrm{W/cm^2}$ [(j)-(l)]. (a), (d), (g) and (j) are evolutions of laser field envelope; (b), (e), (h) and (k) are the phase-space trajectories; (c), (f), (i) and (l) are the power spectra.

ity completely breaks down KAM tori and strong chaos occurs. Irregular HMO crossings exist in phase space [see Figs. 6(h) and (k)], demonstrating the presence of stochastic motions for complex dynamics. The power spectra [Figs. 6(i) and (l)] indicate broadband structures and noiselike spectra being typical of strong chaos. Such strong chaos corresponds to complex patterns with coherence completely broken down, shown in Figs. 7(c) and (d). Figs. 7 (e)-(h) show the evolution of the energy in the first four Fourier modes, in which the system's energy is defined as Eq. (3.3). It shows that coherent, near-coherent and complex patterns are relevant to the stochastic evolution of the energy in the third and fourth modes.

These complicated dynamical phenomena are the characteristic of laser propagation in air. It clearly illustrates that laser filamentation phenomena are associated with the homoclinic chaotic behaviors of laser fields. Furthermore, it shows that the nonlinear dynamical behavior of laser fields depends on the intensity of laser pulses. Physically, the complex pattern of laser filamentation is attributed to the stochastic partition of the system energy in Fourier modes.

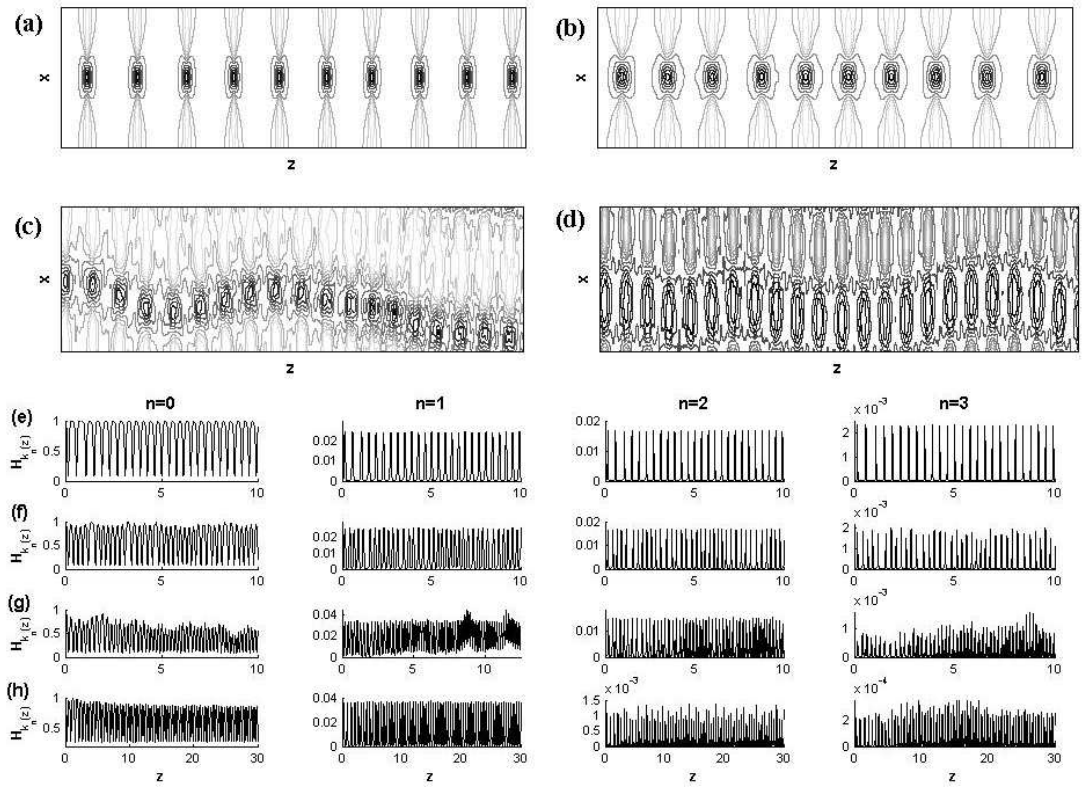

Figure 7: The corresponding complex patterns of laser fields in air [(a)-(d)], and the energy evolution in the first four Fourier modes [(e)-(h)] for the same parameters as Fig. 6.

6 Exponential NSE for medium-intensity laser in underdense plasmas

For a laser pulse with intensity from 10^{15} to $10^{17}\mathrm{W/cm^2}$ interacting with underdense plasmas, considering the Maxwell equations and the electron motion equations, one can also obtain the dimensionless NSE (1.1) in static approximation to describe its dynamics, where the potential function is [10, 11]

$$\text{(iv)} \qquad F(|E|^2)=1-N_e=\frac{1}{2g}(1-e^{-2g|E|^2}). \tag{6.1}$$

Here g is a parameter. When $g=0$, the exponential NSE (ENSE) [Eqs. (1.1) and (6.1)] becomes the above well-known integrable CNSE. The Hamiltonian perturbation here can be written as

$$H_1=\int\left\{\frac{1}{2}|E|^4-\frac{1}{2g}\left[|E|^2+\frac{1}{2g}(e^{-2g|E|^2}-1)\right]\right\}dx. \tag{6.2}$$

where H_0 is also the one (3.2) of CNSE with $\alpha=1$.

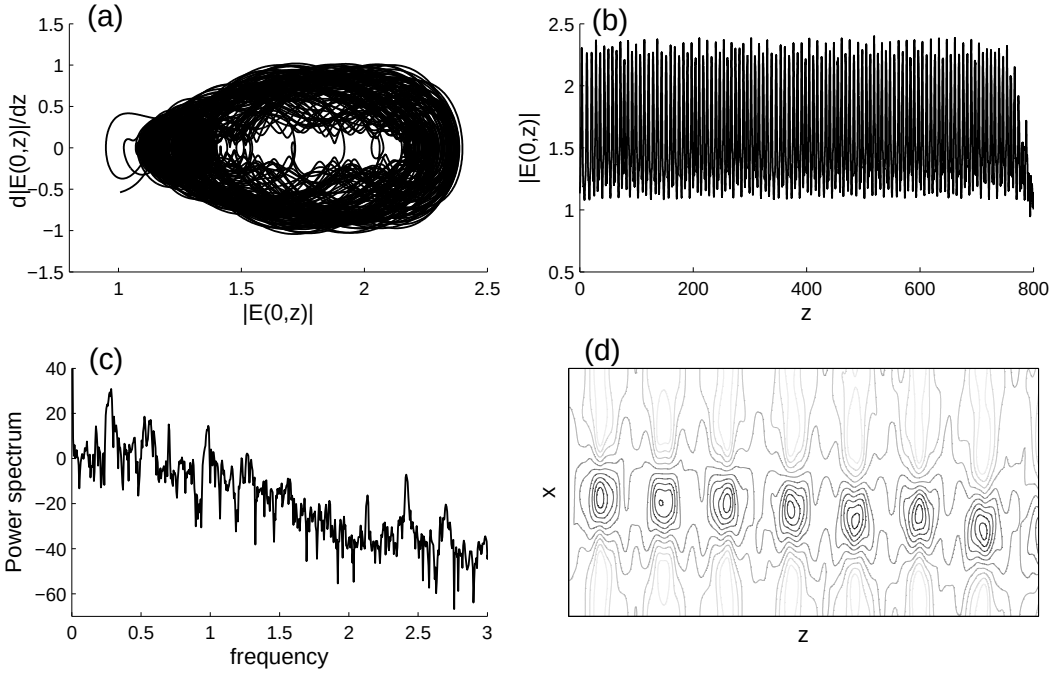

Figure 8: Solutions of Eqs. (1.1) and (6.1) with $\eta=0.1$, $\theta=45^\circ$ and $g=0.1$. (a) phase trajectories illustrate the irregular HMO crossings; (b) propagation of the field amplitude; (c) continuous power spectrum shows the chaotic characteristic; (d) complex patterns with coherence broken down.

In 1994 [11], we also studied the complex dynamics of such laser pulse propagation in plasmas by numerically solving the ENSE [Eqs. (1.1) and (6.1)]. According to the theoretical results obtained in Section 2, the initial condition here should be

$$E_0=\sqrt{(1/2g)l_n(1-2g)^{-1}} \quad \text{for } 0\leq g<\frac{1}{2}$$

and $[\sqrt{(1/2g)l_n(1-2g)^{-1}},0]$ corresponds to a saddle point in phase space. We choose an initial position that lies in the nearby saddle point $(E_0,0)$, that is, $\eta=0.1$, $\theta=45.225^\circ$. For $g=0$, The ENSE [Eqs. (1.1) and (6.1)] becomes a CNSE, the HMO connection is shown in Fig. 1 and the coherent pattern is shown in Fig. 2(d) in Section 3. As $g\neq 0$, however, we find that the stable and unstable manifolds in phase space do not smoothly join together and the irregular HMO crossings exist as shown in Fig. 8(a), which illustrates that the current system is nonintegrable. $|E(0,z)|$ experiences stochastic oscillations [see Fig. 8(b)] with a continuous nonperiodic spectrum [see Fig. 8(c)]. Fig. 8(d) shows the irregular patterns with coherence broken down. Similarly to the above, the irregular patterns are associated with the partition of energy in Fourier modes. As shown in Fig. 9, the energy in the system, which is initially confined to the master mode, would spread to many slaved harmonic modes because of the nonlinear interaction, but would not regroup into the original lowest mode.

To illustrate the route to spatial chaos by the Hamiltonian perturbation H_1 (6.2), we further fix parameters $\theta = 45.225^\circ$, $\eta = 0.1$ and vary g. From Fig. 10, we find the foundational frequency $\omega_0 = 0.2513$ for $g = 0$. When $g = 0.0002$, the wave field still seems to propagate with periodic behavior, but some small peaks in the power spectrum appear and the base frequencies are not uniquely defined. When $g = 0.0008$, in particular, more peaks are produced (but still countable), although the solution does not recur within the finite distance. In a sense, these solutions are called quasiperiodic solutions. With the increase of parameter g, the continuous power spectrum reveals the chaotic behavior (see Fig. 10, in the case of $g = 0.01$, and Fig. 8). From the standpoint of nonlinear dynamics, the base frequency of the cubic NSE is unique (ω_0) for our parameter due to the integrability of the system. However, the nonintegrable perturbation H_1 (6.2) will make the frequency shift, that is, $\omega_i = \omega_0 + \triangle\omega_i$. When the parameter g is quite small, there exist finite countable frequencies. With the increase of g, the oscillatory overlapping of the modes could occur [31], which leads to the formation of the stochastic layer and appearance of the continuous power spectrum.

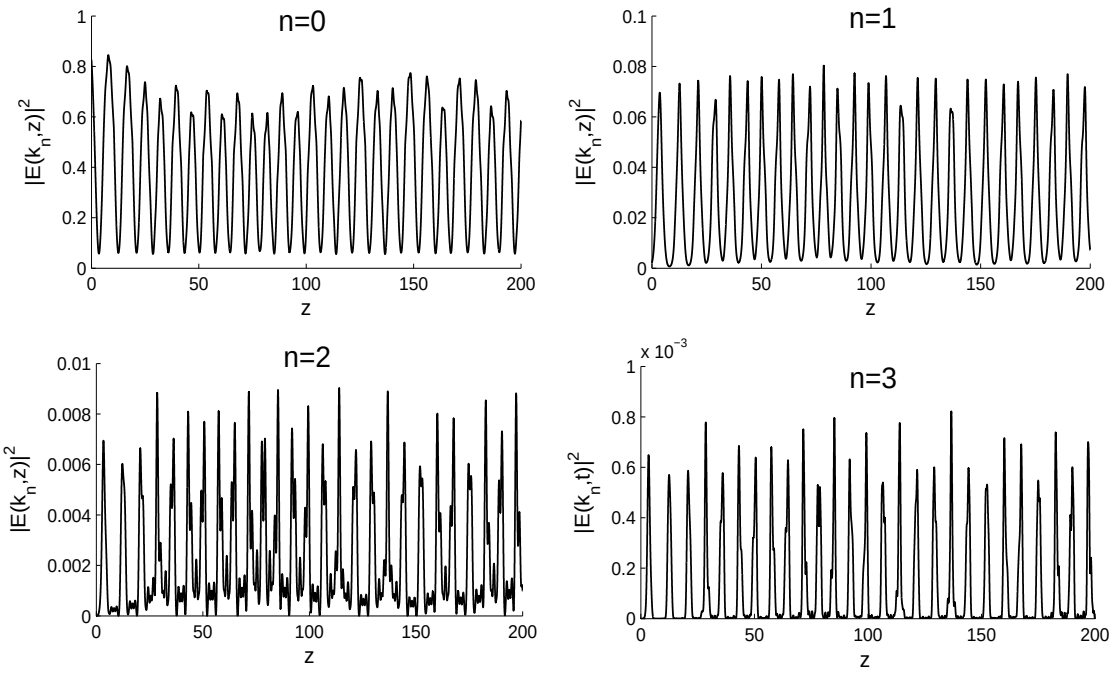

Figure 9: Propagation of energy in the first four Fourier modes, where the parameters are the same as Fig. 8.

In fact, for medium-intensity laser propagation in plasma, the response of the plasma density to the laser fields is only exhibited by the nonlinear ponderomotive force, which corresponds to the exponential nonlinear term in Eq. (6.1). From the investigation, we understand that such a response would act as a nonintegrable perturbation H_1 (6.2) and lead to the stochastic propagation of laser beams.

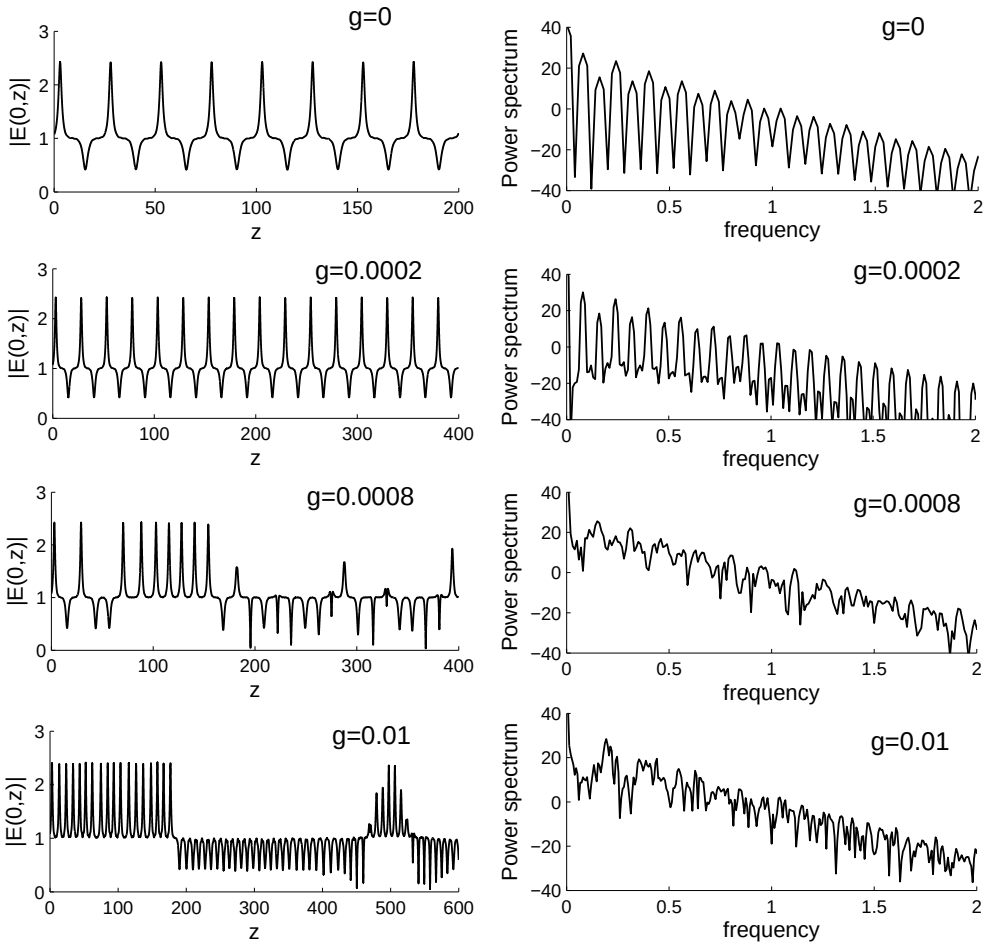

Figure 10: The periodic solution, quasiperiodic solutions, and chaotic solutions for Eqs. (1.1) and (6.1) with $\eta=0.1$ and $\theta=45.225^\circ$. (a) Propagation of the field amplitude; (b) power spectrum.

7 Relativistic NSE for intense laser pulse in plasmas

Interest in the interaction of relativistically intense laser (RIL, at intensities 10^{18} W/cm^2 or above) with plasma has been stimulated by the rapid development of high-power lasers and their applications to fast ignition of fusion fuel, compact X-ray sources and particle accelerators, etc. [23,44,45]. In the RIL the field, electron quiver velocity is highly relativistic and the ponderomotive pressure is much stronger than the plasma pressure. The propagation dynamics of RIL in plasmas are still unclear.

Recently, we [19] also studied the dynamics of RIL in plasmas by using the above method. Considering a circularly-polarized RIL in an initially-homogeneous underdense plasma and introducing the normalizations $E\to m_{e0}\omega cE/e$, $x\to k_p^{-1}x$, and $z\to 2kk_p^{-2}z$, we obtain the RNSE describing the evolution of laser-field envelope [22,46–48], i.e., NSE (1.1)

combined with the potential function

$$\text{(v)} \qquad F(|E|^2)=1-\frac{N_e}{\gamma}=1-\frac{\max[0,1+\partial_x^2\sqrt{1+|E|^2}]}{\sqrt{1+|E|^2}}, \tag{7.1}$$

where the laser intensity is given by $I=(|E|^2\times 1.37\times 10^{18}/\lambda^2)$ W/cm^2. The system (1.1) and (7.1) include the effects of relativistic mass variation and ponderomotive force, as well as diffraction caused by the finite pulse aperture. The Hamiltonian perturbation is

$$H_1=\int\left[\frac{1}{4}|E|^4+2(\sqrt{1+|E|^2}-1)-|E|^2-\left|\partial_x\sqrt{1+|E|^2}\right|^2\right]dx, \tag{7.2}$$

where H_0 expressed as Eq. (3.2) with $\alpha=1/2$ is the integrable Hamiltonian for CNSE. Fig. 11 of $W^{(u)}$ and $W^{(s)}$ manifolds is also completely consistent with the theoretical results in Section 2.

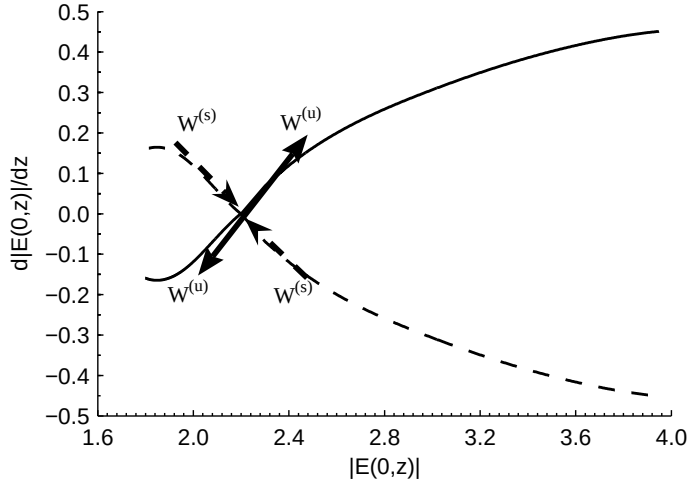

Figure 11: Stable $W^{(s)}$ and unstable $W^{(u)}$ manifolds of the hyperbolic fixed point $(E_0,0)$ with $\theta=45^\circ$ and 225° for the RNSE [Eqs. (1.1) and (7.1)]. The solid curve is for $z>0$ and the dashed curve is for $z<0$.

Physically, the relativistic mass variation and ponderomotive nonlinearities cannot be separated, since they are from the same electron dynamics. However, in order to see their individual contributions to the complexity of the laser-plasma interaction and formation of spatial chaos and patterns, we numerically solve the RNSE [Eqs. (1.1) and (7.1)] with the two cases: (i) the purely relativistic mass variation nonlinearity, and (ii) the combined relativistic mass variation and ponderomotive nonlinearities.

The RNSE [Eqs. (1.1) and (7.1)] with only the relativistic mass variation nonlinearity becomes

$$iE_z+E_{xx}+\left(1-\frac{1}{\sqrt{1+|E|^2}}\right)E=0 \tag{7.3}$$

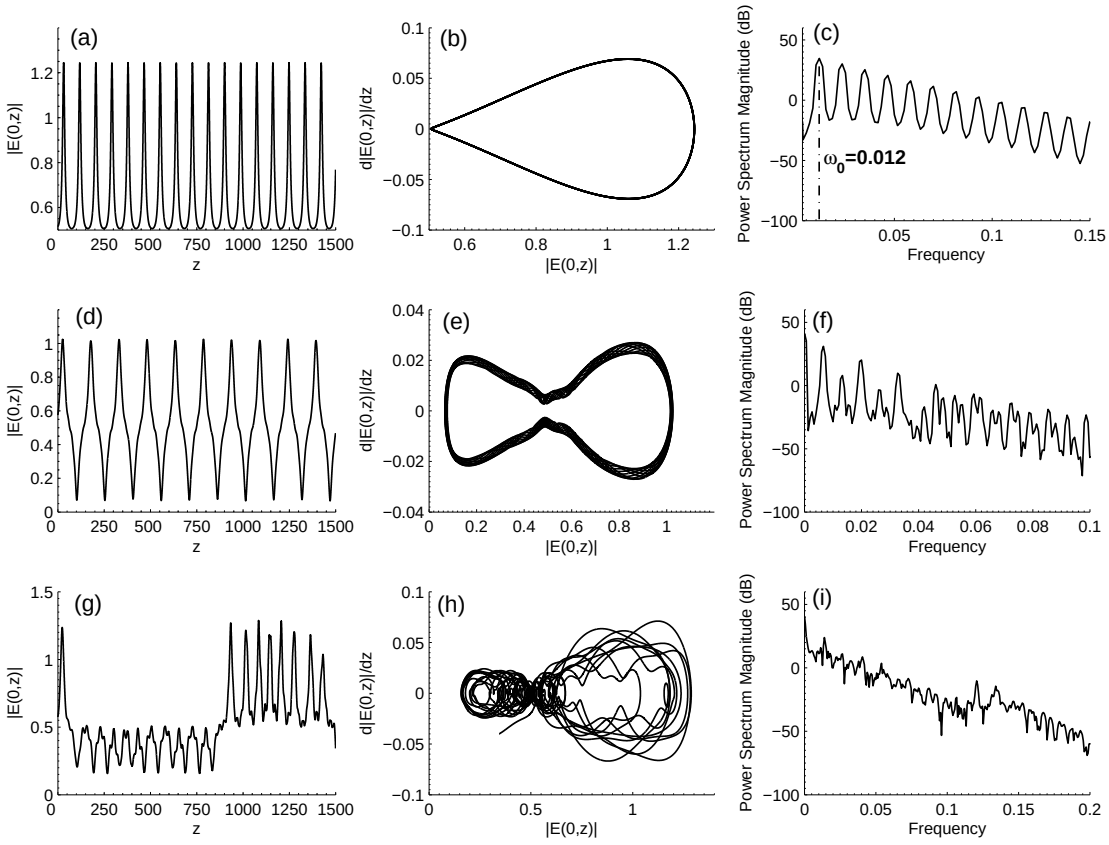

Figure 12: The solutions of the CNSE [(a)-(c)], Eq. (7.3) [(d)-(f)], RNSE [Eqs. (1.1) and (7.1)] [(g)-(i)], for $E_0=0.5$ and $\theta=45^\circ$, at $x=0$. (a), (d), and (g) show the evolution of laser field envelope. (b), (e), and (h) show the structures of the phase space $(E(0,z),\ d|E(0,z)|/dz)$. (c), (f), and (i) show the corresponding power spectra. (h) indicates the irregular homoclinic orbit crossings.

by ignoring the ponderomotive nonlinearity. Eq. (7.3) is physically valid if the condition $k_p^{-2}\nabla^2\gamma\ll 1$ is satisfied [49], where the relativistic nonlinearity prevails over the ponderomotive nonlinearity.

In the weakly relativistic regime with laser intensity $I\leq 1.37\times 10^{18}$ W/cm^2, *i.e.*, $|E|\leq 1$, we can expand Eq. (7.3) to obtain the CNSE [Eqs. (1.1) and (3.1)]. One can then treat the higher-order relativistic mass variation and ponderomotive nonlinearities as Hamiltonian perturbations H_1. We choose parameters $E_0=0.5$ (corresponding to $I_0=6.85\times 10^{17}$ W/cm^2), $\eta=0.1$, and $\theta=45^\circ$. As analyzed in Section 3, the CNSE is fully integrable, one solution corresponding to the periodic oscillations is shown in Figs. 12(a) and (b). However, the integrability breaks down if high-order relativistic mass variation and ponderomotive nonlinearities are taken into account. With the full but only purely relativistic mass variation nonlinearity [Eq. (7.3)], the phase-space trajectory is in the form of a band, the KAM tori becomes thicker but are not completely destroyed [as shown in Fig. 12(e)],

since the solution now contains more subharmonics [see Fig. 12(f)]. This represents a non-chaotic "quasiperiodic" behavior. Under the combined action of the relativistic mass variation and ponderomotive nonlinearities [RNSE's (1.1) and (7.1)], the periodic oscillations disappear and stochastic behavior occurs, as can be seen in Fig. 12(g). On can see from Fig. 12(h) that irregular HMO crossings appear in the phase space. The corresponding dynamical system then is a chaotic one. The power spectra in Fig. 12(i) also shows typical noisy behavior of chaotic motion.

If the laser intensity I is greater than 1.37×10^{18} W/cm^2, corresponding to $|E_0|>1$, both the relativistic mass variation and ponderomotive nonlinearities are important. We use the parameters $E_0=2$ (or $I_0=2.75\times10^{18}$ W/cm^2), $\eta=0.1$, and $\theta=45^\circ$ for numerical calculation. For Eq. (7.3), an interesting phenomenon can be seen in Figs. 13(a) and (b), pseudo-recurrence appears with the laser field exhibiting almost periodic behavior and the phase trajectories are nearly regular with the motion being smooth in small regions. This means that the KAM tori are not completely destroyed by only the relativistic mass variation. However, with both nonlinear relativistic mass variation and ponderomotive effects taken into account [Eqs. (1.1) and (7.1)], the KAM tori are completely destroyed. The laser field envelope displays typical chaotic behavior, as can be seen in Fig. 13(d). Fig. 13(e) shows the irregular HMO crossings in the phase space. Fig. 13(f) shows the broadband structure and the noisy spectra that are typical of chaotic motion.

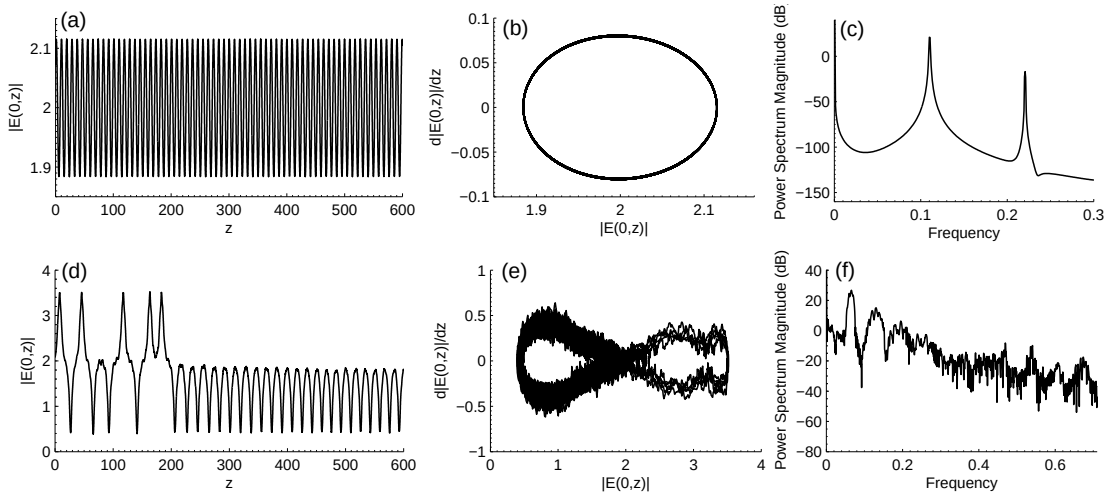

Figure 13: The solutions of Eq. (7.3) [(a)-(c)] and RNSE [Eqs. (1.1) and (7.1)] [(d)-(f)] for $E_0=2.0$ and $\theta=45^\circ$ at $x=0$. (a) and (d) show the evolution of laser field envelope, (b) and (e) show the structures of phase space, (c) and (f) show the power spectra corresponding to (a) and (d), respectively.

The chaotic behavior of the RNSE leads to the appearance of complex patterns for RIL wave field in plasmas. Fig. 14 shows the pattern structures of the CNSE, Eq. (7.3) and the RNSE [Eqs. (1.1) and (7.1)], respectively. With only the fully relativistic mass variation effect, because the KAM tori is not completely destroyed and laser field evolution is only weakly chaotic, its pattern structure in general remains fairly coherent, but irregular sub-

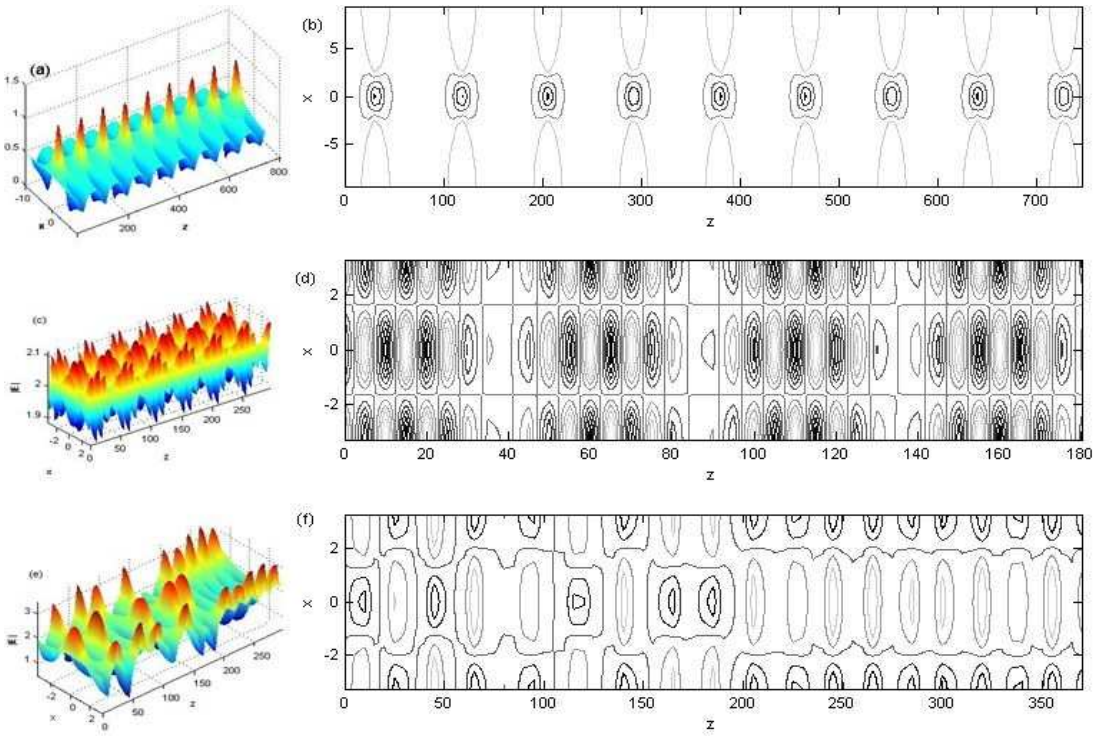

Figure 14: Spatial patterns: (a) and (b) show the coherent patterns of the CNSE for $E_0=0.5$ and $\theta=45^\circ$, (c) and (d) show the nearly coherent patterns of Eq. (7.3) with only the relativistic mass variation effect, and (e) and (f) show the complex patterns of the RNSE [Eqs. (1.1) and (7.1)] with both the relativistic mass variation and ponderomotive nonlinearities, for $E_0=2.0$ and $\theta=45^\circ$.

structures appear, as shown in Figs. 14(c) and (d). This near-coherent behavior can also be seen in Figs. 15(b): the energy evolution is periodic in the first two Fourier modes, but aperiodic in the third and fourth modes. With both the fully relativistic mass variation and ponderomotive nonlinearities, the KAM tori are completely destroyed and strong chaos occurs. The corresponding complex patterns can be seen in Figs. 14(e) and (f). The localized structures remain but they are rather irregular. Fig. 15(c) shows that the evolution of the energy in the first mode is quasi-periodic, so that spatially localized structures remain. However, the evolution of the energy in the second and higher modes exhibits stochastic, resulting in irregular complex patterns.

All these show that the relativistic mass variation and ponderomotive nonlinearities in the RNSE (7.1) lead to the chaotic behaviors of laser fields. Coherent structures are replaced by complex patterns, HMO crossings exist in the phase space and stochastic partition of energy in Fourier modes occurs. Furthermore, the ponderomotive nonlinearity plays a more important role in completely destroying the periodicity of laser field and forming chaos and complex patterns. With only the relativistic mass variation nonlinearity, laser field tends to remain pseudo-periodic with pseudo-recurrent phase orbit, and the patterns remain fairly coherent.

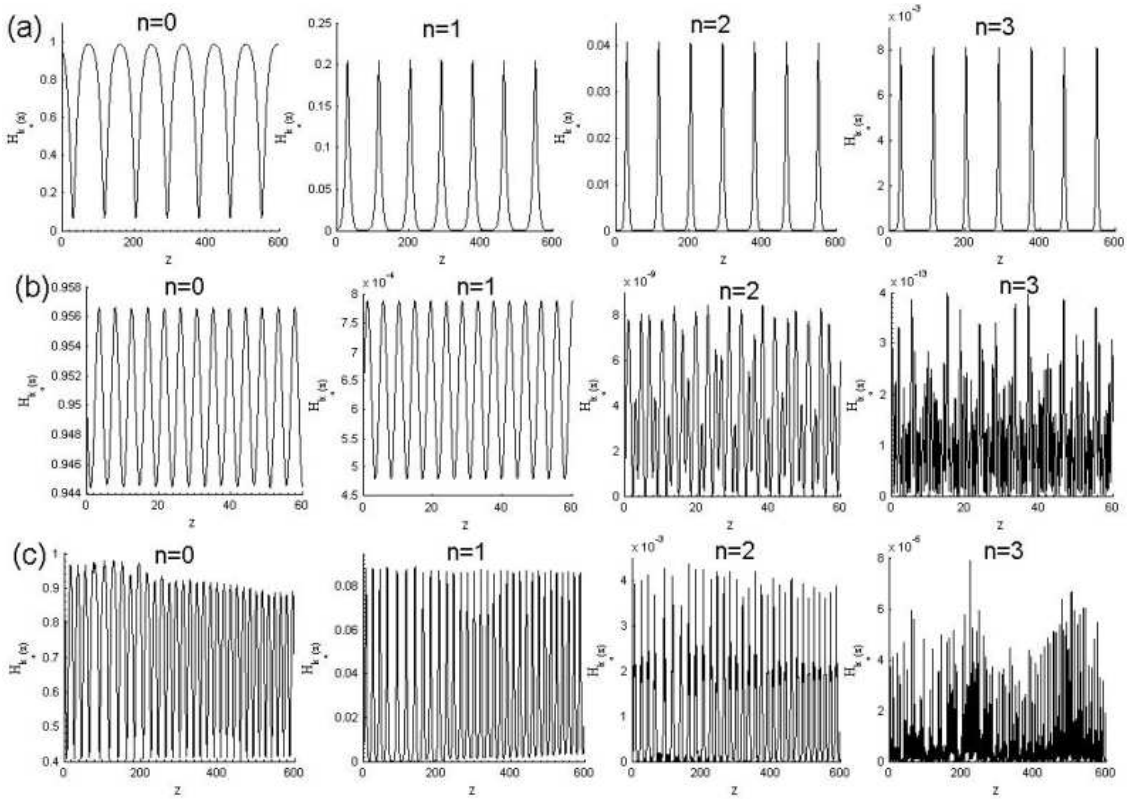

Figure 15: Energy evolution of the first four Fourier modes for the CNSE, Eq. (7.3), and RNSE [Eqs. (1.1) and (7.1)] The parameters are the same as in Fig. 14.

8 Conclusion and discussion

We have given a systematic review of the complex dynamics including chaos and patterns of a series of generalized NSEs with different potential functions for various nonlinear physical problems in plasmas. Our studies from the early Langmuir wave turbulence to the recent laser filaments in plasmas all show that the high-order nonlinear effects, acting as the Hamiltonian perturbation, break down the NSE integrability and lead to the chaotic behaviors of the system. The corresponding nonlinear phenomena are just associated with this homoclinic chaos. In particular, we found that the unstable manifolds $W^{(u)}$ possessing the hyperbolic fixed point correspond to an initial phase θ=45° and 225°, and the stable manifolds $W^{(s)}$ correspond to θ=135° and 315°. We believe these findings are general and will give useful implication to the understanding of nonlinear wave and laser propagation dynamics in plasmas.

As far as various branches of physics are concerned, the presence of the stochastic wave fields (Langmuir wave field or laser wave field) depends on the evolution processes of systems. In other words, the lowest order nonlinear term $|E|^2E$ is the predominant

nonlinear mechanism in the evolving initial stages. Some important phenomena, such as coherent structures and Langmuir wave collapse, etc., can be reasonably explained by making use of the cubic NSE. In the strongly nonlinear stages, other physical effects could play an important role in the process of plasma instabilities. For example, Landau damping of high-frequency waves, $\chi^{(5)}$ susceptibility, multiphoton ionization, relativistic ponderomotive force and so on become quite significant in different problems. These higher-order nonlinear effects make complex dynamic behaviors occur. In a sense, these complex dynamic phenomena are the characteristic of wave propagation. It is shown that the focusing (or collapse) of wave becomes a chaotic oscillation, rather than a catastrophic process due to the higher-order nonlinear effects. Moreover, the latter acts not only as a locally saturating nonlinearity, but also as a global Hamiltonian perturbation resulting in complex propagation dynamics.

Acknowledgments

B.Q. acknowledges the financial support of Department of Physics, National University of Singapore. CTZ would like to thank the great hospitality of the Temasek Laboratories of National University of Singapore, where part of work was performed during his visits. This work is also supported by the National Natural Science Foundation of China grant Nos. 10575013 and 10576007, and partially by the National Basic Research Program of China (973) (2007CB814802 and 2007CB815101).

References

[1] X. T. He, Acta Phys. Sin. 30, 1415 (1981).
[2] X. T. He, Acta Phys. Sin. 31, 1317 (1982).
[3] C. T. Zhou, X. T. He, S. G. Chen, Phys. Rev. A 46, 2277 (1992), also the references therein.
[4] C. T. Zhou, S. P.Zhu, X. T. He, Phys. Rev. A 46, 3486 (1992).
[5] X. T. He, C. T. Zhou, J. Phys. A 26, 4123 (1993).
[6] C. T. Zhou, X. T. He, Comm. Theor. Phys. 19, 231 (1993).
[7] C. T. Zhou, X. T. He, Chinese Phys. Lett. 10, 290 (1993).
[8] C. T. Zhou, X. T. He, Mod. Phys. Lett. B 8 1503 (1994).
[9] C. T. Zhou, X. T. He, Phys. Scr. 50, 415 (1994).
[10] C. T. Zhou, X. T. He, Phys. Rev. E 49, 4417 (1994).
[11] C. T. Zhou, X. T. He, T. X. Cai, Phys. Rev. E 50, 4136 (1994).
[12] C. T. Zhou, C. H. Lai, Int. J. Mod. Phys. C 7, 775 (1996).
[13] X. T. He, C. Y. Zheng, Phys. Rev. Lett. 74, 78 (1995).
[14] Y. Tan, X. T. He, S. G. Chen, Phys. Rev. A 45, 6109 (1992).
[15] C. Y. Zheng, X. T. He, Y. Tan, Modern Phys. Lett. B 8, 833 (1994).
[16] C. T. Zhou, M. Y. Yu, X. T. He, Phys. Rev. E 73, 026209 (2006).
[17] C. T. Zhou, Chaos 16, 013124 (2006).
[18] B. Qiao, C. H. Lai, C. T. Zhou, X. T. He, X. G. Wang, Appl. Phys. Lett. 91, 221114 (2007).
[19] B. Qiao, C. H. Lai, C. T. Zhou, X. T. He, X. G. Wang, Phys. Plasmas 14, 112301 (2007).

[20] See for example, Y. S. Kivshar, G. P. Agrawal, Optical Solitons: From Fibers to Photonic Cryptals, Academic Press, London, 2003.
[21] K. Okamota, Fundamentals of Optical Waveguides, Academic Press, London, 2000.
[22] A. V. Borovsky, A. L. Galkin, A. B. Shiryaev, T. Auguste, Laser Physics at Relativistic Intensities, Springer, Berlin, 2003.
[23] P. Gibbon, Short Pulse Laser Interactions with Matter - An Introduction, Imperial College Press, London, 2005.
[24] P. L. Kelley, Phys. Rev. Lett. 15, 1005 (1965).
[25] M. J. Alblowitz, H. Segur, J. Fluid Mech. 93, 691 (1979).
[26] T. Taninuti, H. Washimi, Phys. Rev. Lett. 21, 209 (1968).
[27] A. I. Olemskoi, V. F. Klepikov, Phys. Reports 338, 571 (2000).
[28] F. T. Arecchi, S. Boccaletti, P. L. Ramazza, Phys. Reports 318, 1 (1999).
[29] A. S. Mikhailova and K. Showalterb, Phys. Reports 425, 79 (2006).
[30] T. H. Moon, Phys. Rev. Lett. 64, 412 (1990).
[31] A. J. Lichtenberg, M. A. Lieberman, Regular and Chaotic Dynamics, Springer, New York, 1992, pp. 1-20.
[32] C. T. Zhou, C. H. Lai, M. Y. Yu, J. Math. Phys. 38, 5225 (1997); Phys. Scr. 55, 394 (1997).
[33] G. M. Zaslavsky, R. Z. Sagdeev, D. A. Usikov, A. A. Chernikov, translated by A. R. Sagdeeva, Weak Chaos and Quasi-Regular Patterns, Cambridge University Press, Cambridge, 1991, pp. 21-35 and pp. 86-108.
[34] C. Sulem, P. Sulem, The Nonlinear Schröinger Equation: Self-focusing and Wave Collapse, Springer, Berlin, 2000.
[35] A. Hasegawa, Optical Solitons in Fibers, Springer-Verlag, Berlin, 1989.
[36] A. Alexandrescu, G. D. Montesinos, V. M. Pérez-García, Phys. Rev. E 75, 046609 (2007).
[37] T. B. Benjamin, J. E. Feir, J. Fluid Mech. 27, 417 (1967).
[38] A. Cloot, B. M. Herbst, J. A. C. Weideman, J. Comput. Phys. 86, 127 (1990)
[39] B. J. Lemesnrier, G. Papanicollaon, C. Sulem, P. L. Sulem, Physica D 31, 79 (1988).
[40] R. Ackermann, E. Salmon, N. Lascoux, J. Kasparian, P. Rohwetter, K. Stelmaszczyk, S. Li, A. Lindinger, L. Wöste, P. Béjot, L. Bonacina, J. P. Wolf, Appl. Phys. Lett. 89, 171117 (2006).
[41] K. Stelmaszczyk, P. Rohwetter, G. Méjean, J. Yu, E. Salmon, J. Kasparian, R. Ackermann, J. P. Wolf, L. Wöste, Appl. Phys. Lett. 85, 3977 (2004).
[42] L. Wöste C. Wedekind, H. Wille, P. Rairoux, B. Stein, S. Nikolov, Ch. Werner, S. Niedermeier, H. Schillinger, R. Sauerbrey, Laser Optoelektron 29, 51 (1997).
[43] L. Bergé, S. Skupin, F. Lederer, G. Méjean, J. Yu, J. Kasparian, E. Salmon, J. P. Wolf, M. Rodriguez, L. Wöste, R. Bourayou, R. Sauerbrey, Phys. Rev. Lett. 92, 225002 (2004), also the references therein.
[44] C. T. Zhou and X. T. He, Appl. Phys. Lett. 90, 031503 (2007); ibid. 92, 071502 (2008); ibid. 92, 151502 (2008); Opt. Lett. 32, 2444 (2007).
[45] C. T. Zhou, M. Y. Yu, X. T. He, J. Appl. Phys. 101, 103302 (2007); Europhys. Lett. 79, 35001(2007); Laser Part. Beam 25, 313 (2007); Phys. Plasmas 13 092109 (2006).
[46] G. Z. Sun, E. Ott, Y. C. Lee, P. Guzdar, Phys. Fluids 30, 526 (1987).
[47] A. B. Borisov, O. B. Shiryaev, A. McPherson, K. Boyer, C. K. Rhodes, Plasma Phys. Control. Fusion 37, 569 (1995).
[48] M. Y. Yu, P. K. Shukla, K. H. Spatschek, Phys. Rev. A 18, 1591 (1978).
[49] P. Sprangle, A. Zigler, E. Esarey, Appl. Phys. Lett. 58, 346 (1991).